Spontaneous fast-ultradian dynamics of polymorphic interictal events in drug-resistant focal epilepsy

Damian Dellavale, Francesca Bonini, Francesca Pizzo, Julia Makhalova, Fabrice Wendling, Jean-Michel Badier, Fabrice Bartolomei, Christian-George Bénar

Pizzo Francesca (Orcid ID: 0000-0001-6345-1288)
Makhalova Julia (Orcid ID: 0000-0001-7962-2942)
Bartolomei Fabrice (Orcid ID: 0000-0002-1678-0297)
Dellavale Damián (Orcid ID: 0000-0003-0472-8472)

Spontaneous fast-ultradian dynamics of polymorphic interictal events in drug-resistant focal epilepsy

Damián Dellavale[1, 2], Francesca Bonini[1, 3], Francesca Pizzo[1, 3], Julia Makhalova[1, 3], Fabrice Wendling[4], Jean-Michel Badier[1], Fabrice Bartolomei[1, 3], Christian-George Bénar[1]

[1] Aix Marseille Univ, INSERM, INS, Inst Neurosci Syst, Marseille, France.

[2] Centro Atómico Bariloche and Instituto Balseiro, CONICET, CNEA, UNCUYO, R8402AGP San Carlos de Bariloche, Río Negro, Argentina.

[3] APHM, Timone hospital, Epileptology and cerebral rythmology, Marseille, France.

[4] Université de Rennes 1, INSERM, LTSI-U1099, Campus de Beaulieu, F-35000, Rennes, France.

Correspondence

Damián Dellavale (dellavale@cab.cnea.gov.ar)

Christian-George Bénar (christian.benar@univ-amu.fr)

Epileptology and Cerebral Rhythmology, Timone Hospital, Public Assistance Hospitals of Marseille, 264 Rue St Pierre, Marseille 13005, France.

Acknowledgments

This article has been accepted for publication and undergone full peer review but has not been through the copyediting, typesetting, pagination and proofreading process which may lead to differences between this version and the Version of Record. Please cite this article as doi: 10.1111/epi.17655

This work was supported by the ANR Neurosense ANR-18-CE19-0013 grant, and by the RHU EPINOV [A*MIDEX project (ANR-17-RHUS-0004) funded by the 'Investissements d'Avenir' French Government].

Authors contribution

DD contributed to the conceptualization, methodology, formal analysis, writing the original draft and figures preparation. FBo, FP, CGB and FB contributed to the data acquisition and visual analysis of the recordings, review and editing the manuscript. JM contributed to the acquisition and curation of the dataset. FW, JMB, FB, CGB contributed to the funding acquisition.

Disclosure of Conflicts of Interest

None of the authors has any conflict of interest to disclose.

Ethical Publication Statement

We confirm that we have read the Journal's position on issues involved in ethical publication and affirm that this report is consistent with those guidelines.

Data availability

The data and code that support the findings of this study are available from the corresponding author, upon reasonable request. In particular, the source code for the computation of the NODE algorithm together with test script examples are freely available at https://github.com/damian-dellavale/node/

We are willing to provide technical support to investigators who express an interest in implementing the NODE algorithm in other programming languages, integrate it in open-source software toolboxes, or use it for non-profit research activities.

Abstract

Objective

We studied the rate dynamics of interictal events occurring over fast-ultradian time scales, as commonly examined in clinics to guide surgical planning in epilepsy.

Methods

Stereoelectroencephalography (SEEG) traces of 35 patients with good surgical outcome (Engel I) were analyzed. For this, we developed a general data mining method aimed at clustering the plethora of transient waveform shapes including interictal epileptiform discharges (IEDs), and assessed the temporal fluctuations in the capability to map the epileptogenic zone (EZ) of each type of event.

Results

We found that the fast-ultradian dynamics of the IEDs rate may effectively impair the precision of EZ identification, and appear to occur spontaneously, that is, not triggered by or exclusively associated with a particular cognitive task, wakefulness, sleep, seizure occurrence, post-ictal state or antiepileptic drug withdrawal. Propagation of IEDs from the EZ to the propagation zone (PZ) could explain the observed fast-ultradian fluctuations in a reduced fraction of the analyzed patients, suggesting that other factors like the excitability of the epileptogenic tissue could play a more relevant role. A novel link was found between the fast-ultradian dynamics of the overall rate of polymorphic events and the rate of specific IEDs subtypes. We exploited this feature to estimate in each patient the 5 min interictal epoch for near-optimal EZ and resected zone (RZ) localization, which resulted at the population level better than those obtained using either 1) the whole time series available in each patient ($P = 0.084$ for EZ, $P < 0.001$ for RZ, Wilcoxon signed rank test) and 2) 5 min epochs randomly sampled from the interictal recordings of each patient ($P < 0.05$ for EZ, $P < 0.001$ for RZ, 10^5 random samplings).

Significance

Our results highlight the relevance of the fast-ultradian IEDs dynamics in mapping the EZ, and show how it can be prospectively estimated to inform surgical planning in epilepsy.

Keywords

Stereo EEG dynamics, Epileptogenic biomarkers, Epileptiform spike subtypes, Neural tissue excitability, Nested outlier detection, Local false discovery rate.

Key Points

- The rate of IED observed in SEEG recordings undergoes spontaneous fluctuations over fast-ultradian time scales.
- The fast-ultradian dynamics of the IED rate may impair the EZ identification and hence are clinically relevant for surgical planning.
- Propagation does not fully explain the fast-ultradian dynamics of the IED rate constraining the precision to localize the EZ.
- Interictal epochs, as commonly examined in clinics, producing near-optimal EZ mapping can be inferred based solely on the LFP dynamics.
- Fluctuations of the AUPREC based on epileptic and non-epileptic events are linked to scale-free and scale-rich processes, respectively.

Introduction

The success rate of the surgical treatment for drug-resistant focal epilepsies is in the order of 60%.[1,2] This imperfect outcome can be partially explained by the fact that optimal delineation of the

epileptogenic zone (EZ) remains unknown. In this context, significant efforts are being made to quantify intracranial EEG[3] and extract biomarkers that can best predict the location of the EZ. Epileptic spikes are the classic interictal biomarker of epilepsy, used by epileptologists as part of standard practice to inform surgical planing.[4] The relationship of the EZ with the epileptiform spikes is complex. In a previous study it was shown a variable correlation of the spike rate with EZ, but particularly important in focal cortical dysplasia.[5] Currently, there is no gold standard to define subtypes of epileptiform discharges and to differentiate them from non-epileptic paroxysmal events.[6] However, some characteristics of spikes have been found to be better markers of EZ, such as frequency of occurrence, association with high frequency oscillations (HFO)[7,8] or with gamma activity.[9] An underestimated dimension is the time-varying factors underlying the genesis of different subtypes of interictal epileptiform discharges.[10] In this regard, there are important open issues related to the way IEDs fluctuate in spatial extent,[11] waveform shape (see Figure 2A in Tomlinson et al.[12]) and rate of occurrence. The temporal dynamics of IEDs expand over a wide range of time scales, from milliseconds associrks[12,13] to circadian
(day) and even multidien (week/month) fluctuations in relation to sleep and ictogenesis among other factors.[14-18] Therefore, the integration of all available information over a broad range of spatial and temporal scales is crucial to improve the EZ localization based on interictal SEEG recordings.
In this work we report on a quantitative analysis of the fluctuations of the IEDs rate over fast-ultradian time scales, as well as the impact of such temporal fluctuations on the capacity of IEDs to map the EZ. The fast-ultradian dynamics analyzed in our work refers to temporal fluctuations of the rate of interictal events, not necessarily periodic, expanding over time scales ranging from sub-minute up to half an hour (i.e. sub-hour temporal dynamics).[19] In particular, we focus on the study of previously unexplored IEDs rate dynamics of spontaneous nature and occurring in SEEG recordings as commonly examined in clinics to inform surgical planning in epilepsy (in the range of 5 minutes to 2 hours of SEEG recordings). We developed a general data mining method aimed at clustering the plethora of transient waveform shapes emerging in interictal SEEG recordings (referred in this study as polymorphic interictal events), and assessed the fluctuation in predictive power of each type of

event. Importantly, the proposed method for polymorphic events analysis paves the way to unveil a novel and counter-intuitive link between the dynamics of the overall rate of polymorphic events and the rate of specific subtypes of epileptiform spikes which is exploited here to improve the EZ localization.

Methods

Patients and intracerebral recordings

Patients with drug resistant focal epilepsy were selected from the database of the Epileptology Unit of La Timone Hospital based on the outcome of the resective surgery. The final study includes 35 patients (20 women and 15 men) with Engel I seizure outcome classification at least 12 months after the surgical procedure, identified in the period 2008 to 2019. A variety of pathologies and electrode coverages were represent SEEG surgery was 27 years (range = 19.5 - 41 years). Written informed consent regarding the SEEG procedure was obtained from all individual participants included in the study. In all patients, indication for SEEG exploration was based on Phase I presurgical non-invasive assessments for pharmacoresistant focal epilepsy including examination of detailed clinical history, neurological evaluation,neuropsychological testing, long-term scalp video-EEG monitoring and high -resolution structural magnetic resonance imaging (MRI). SEEG exploration was performed using intracerebral electrodes(Dixi Medical or Alcis Neuro (France); 10 - 15 contacts, length: 2 mm, diameter: 0.8 mm, 1.5 mm

apart), placed intracranially according to Talairach stereotactic method[20]. The anatomical targets for electrode placement were defined based on the hypotheses about EZ localization resulting from Phase I. A postoperative computed tomography (CT) scan and/or MRI was performed to verify the spatial accuracy of the implantation. CT/MRI data coregistration was performed to check the anatomical location of each contact along the electrode trajectory. Local field potentials (LFP) from the SEEG electrodes were recorded on a 128-channel system (Natus/Deltamed) sampled at 512 Hz or

1024 Hz (16 bits resolution), with a built-in hardware high-pass filter (cutoff frequency = 0.16 Hz) and an antialiasing low-pass filter (cutoff frequency = 170 Hz for 512 Hz sampling rate, or 340 Hz for 1024 Hz sampling rate). Video-SEEG recordings were performed as long as necessary (1 - 3 weeks) to record several of the patient's habitual seizures. Long term video-SEEG recordings following withdrawal of antiepileptic drugs were judged to be necessary to delineate the localization of the epileptogenic zone (EZ) for surgical treatment. The SEEG recordings analyzed in this work were chosen at least 2 days after the electrode implantation surgical procedure, and when possible before medication tapering, to limit possible effects of general anesthesia and antiepileptic drug withdrawal. In addition, we selected interictal recordings that were temporally distant from the preceding and the following seizure by at least 2 hs. The SEEG traces were recorded during time intervals in which the patients were either awake at rest or during non-REM sleep. For the awake state at rest, the patients were instructed to remain awake and during the SEEG recordings they were laying in bed doing nothing (not engaging in any particular cognitive task). Some patients, in particular the ones corresd have undergo drowsy(not sleep) state during part of the recording time interval. In all the cases, the patient state (awake at rest or non-REM sleep) was confirmed by the dedicated staff who reviewed the SEEG traces and the video monitoring the patient during the intracerebral recordings. Unless otherwise indicated, the results presented in this work correspond to the 35 patients listed in Table 1 and S1 for the awake state at rest. The results corresponding to the non-REM sleep are presented and discussed in Appendix S1, Section 11. In order to compare the results between two SEEG recording sessions taken at different days and time of day for the same patient state (awake at rest), a second group of

12 patients are presented and discussed in Appendix S1, Section 12. Not all the patients included in this second group have Engel I seizure outcome (see Table S2). The epileptologists team performed a visual evaluation of the SEEG traces before the analysis to identify interictal periods with a limited amount of artifacts (see Table S1). The median time-length of the interictal SEEG traces among the 35 patients in awake state was 28.2 min, range = 23.5 - 31.6 min (see Table S1). The classification of the SEEG contacts in EZ, propagation zone (PZ) and non-involved zone (NIZ) was made according

to the sites of seizure initiation (SOZ) based on visual analysis and on the Epileptogenicity Index (EI).[4,5,21] Further details about the classification of the SEEG contacts can be found in the Appendix S1, Section 1. Across the 35 patients included in the Table 1, a total of 428 brain regions were analyzed (median per patient = 13, range = 11 - 14). There were a total of 5154 SEEG contacts, 962 in epileptogenic zone (EZ), 904 in propagation zone (PZ), 3288 in non-involved zone (NIZ) and 1486 in the resected zone (RZ). The SEEG macroelectrode contacts were converted to a bipolar referencing montage for subsequent analysis. Bipolar channels were obtained as the difference between signals recorded from spatially adjacent contacts pertaining to the same depth electrode array. For other clinical characteristics of the patients see Table 1.

Data and statistical analysis

To systematically study the variety of transient waveform shapes emerging in the interictal SEEG dynamics, we developed a general data mining
method. The NODE algorithm uses the Local False Discovery Rate (LFDR) method[22,23] to define the interictal events by detecting anomalies (i.e. outliers) of amplitude across the frequency bands of interest. Figure 1A schematizes the main processing steps associated with the NODE algorithm. Briefly, the NODE algorithm assigns to each event a 4-digit label. Each label digit represents the proportion of the detected anomalies that can be expected to be true outliers in the frequency band associated with that digit. The four frequency bands range from High-Delta band corresponding to the first label digit from the left, to Ripple band corresponding to the last label digit from the left. For instance, the label 0_09_09_0 groups all the interictal events with a proportion of 90% of them that can be expected to have true outliers in the two medium frequency bands [8 Hz - 32 Hz] and [30 Hz - 155 Hz]. The label 0_09_09_05 groups sharper transient waveform shapes since these paroxysmal events have, in addition to the outliers in the two medium frequency bands, a proportion of 50% of the detected anomalies associated with the Ripple band [150 Hz - 255 Hz] of these events that can be expected to be true outliers (see Figure 1C). The label 09_09_09_05 groups the spike-wave

complexes with a proportion of 90% of them that can also be expected to have true outliers in the low frequency band [1 Hz - 10 Hz] corresponding to the first label digit from the left (see Figure 1B). Further details about the NODE algorithm and the semi-supervised constrained clustering method,[24] can be found in the Appendix S1, Section 2. Time-frequency maps of the polymorphic events were computed as scalograms using Morlet wavelets (see Appendix S1, Section 3).[25] To quantify the capability of the subtypes of events identified by the NODE algorithm in segregating the SEEG channels involved in the epileptogenic zone (EZ) from those not involved (NIZ), we implemented a precision and recall analysis which is a suitable tool for imbalanced classification problems (see Appendix S1, Section 4). To compare distributions of paired samples we used a two-tailed non-parametric Wilcoxon signed rank test with $\alpha = 0.05$. A non-parametric permutation test based on random sampling without replacement was used for non-paired group analysis. Unless otherwise indicated, all the reported P values were Bonferroni-adjusted to correct for multiple comparisons. In all the violin plots, center gray boxes represent the 25th and 75th percentiles, whiskers (gray lines) extend to the most extre he interquartile range(IQR)), star markers represent outliers. The center white circle and white line indicate the median
and mean, respectively. For further details about the methods used to characterize the fast-ultradian dynamics associated with the interictal events rate, the reader is referred to the Appendix S1, Sections 5 and 6.

Results

Detection and clustering of interictal events

We used the NODE algorithm to detect and cluster interictal events by identifying amplitude outliers across two LFDR thresholds and four frequency bands, with a time discretization of 200 ms defining the time length of each event (see Figure 1A). The variety of the detected interictal events expanded over the maximum number of clusters corresponding to this particular set of NODE parameters (80

clusters, each one characterized by 4-digit label). In the detection and clustering stages, we followed a epileptogenicity-agnostic approach, that is, no *a priori* information about the epileptogenic or physiological nature of the events was introduced during the detection and labeling processes. Then, to assess the epileptogenicity of the detected events we implemented two quantitative strategies, 1) ordering the NODE clusters according to their power to segregate the EZ and NIZ channels across all the patients (see Figure S1), and 2) computing the fraction of epileptiform discharges as visually identified by an epileptologist (FBo) captured by each NODE cluster (see Figure S3). Importantly, consistency was found between these two approaches (see Figures S1 and S3). Figures 1B, 1C and 1D show examples of two subtypes of IEDs given by the clusters 0_09_09_05 and 09_09_09_05 which were associated by the epileptologists with interictal epileptiform spikes and spike-wave complexes respectively, and one type of non-epileptiform events associated with amplitude outliers occurring in the low frequency bands (1 Hz - 30 Hz, Cluster: 09_0_0_0). Interestingly, we found that the events corresponding to low frequency oscillations (e.g. Clusters: 09_0_0_0) were significantly less abundant in the EZ cthe analyzed patients(see Figures S1C and S1D). Henceforth, we will refer to the events grouped in these clusters as non-epileptic events. Figure S3 shows that only a small fraction of the visually marked spikes

corresponds to NODE clusters which were found to be significantly more abundant in NIZ than in EZ across the 35 patients included in the Table 1 (e.g. cluster 0_09_0_0 in Figures S1 and S3). This observation is consistent with the notion that primary spikes associated with EZ and/or abnormal activity have sharper waveform shapes, meaning their spectral decomposition shows more power in the high frequency bands (e.g. clusters 09_09_09_05, 0_09_09_05), when compared to other discharges having smoother waveform morphologies (e.g. cluster 0_09_0_0) which can be in part explained by a propagation mechanism.[5,12,28-30] Figure 1E, 1F and 1G show the mean rate of events (average over 60 min recording) in each bipolar channel of the patient 7, together with the results of the precision and recall analysis quantifying the capacity of EZ localization associated with each type of event. Importantly, it was found that the subtypes of sharp paroxysmal events identified by the NODE algorithm present important differences in terms of their capacity for the localization of the

epileptogenic zone (EZ). In particular, for the patient 7 the clusters 09_09_09_05, 0_09_09_05 and 09_09_09_0 produce F1 max = 0.93, F1 max = 0.73 and F1 max = 0.64 for EZ localization, respectively (see Figures 1E, 1F and Figure S1A). The Figure S1C shows the quantification of the capacity for EZ localization of the 80 NODE clusters across all the analyzed patients.

Spontaneous fast-ultradian dynamics of the rate of interictal events

We then investigated the temporal dynamics of the interictal events, not necessarily periodic, expanding over time scales ranging from sub-minute up to half an hour (i.e. sub-hour temporal dynamics). For this, we analyzed SEEG recordings as commonly examined in clinics for the treatment of drug-resistant epilepsy (in the range of 5 minutes to 2 hours of SEEG recordings).[5,8,9,26,27]

Figures 2A and 2B show for two patients (7, 13) the cumulative count of all the detected events (CE) across the SEEG channebipolar channel). In

these plots, the slope of each rectilinear segment correspond to the mean rate of events in that particular bipolar channel (total number of events / whole time period shown in the figures). In order to analyze the fluctuations of the events rate around its mean value, we subtracted a fitted straight line from the CE to obtain the residuals of the CE for each bipolar channel. The resulting detrended count of events (DCE) are presented in Figures 2C and 2D showing a clear oscillatory dynamics of the DCE in particular for the bipolar channels pertaining to the EZ. In the Figures 2C and 2D, the time intervals of the DCE with positive or negative slope correspond to an increase or decrease of the instantaneous rate of events, respectively. Significantly, we found that the interictal dynamics of the rate of polymorphic events observed over fast-ultradian time scales was highly independent of the parameters used in the NODE algorithm (see Figures S4, S5 and S6) and also independent of the specificity of the events detector (compare the fluctuations disclosed by the clusters 0_09_09_05 and 09_09_09_05 with respect to the Spike-like group in the Figures 3A to 3D). These results suggest that the observed dynamics is an intrinsic feature of the interictal neural activity captured by the

SEEG recordings, putatively elicited by physiological brain states and/or epileptogenic mechanisms. Then, we analyzed whether the temporal fluctuations of the DCE during the analyzed fast-ultradian time scales entrain the rate of specific epileptogenic biomarkers or not, which could ultimately affect the localization of the EZ. To investigate this, we focused on the temporal evolution of the rate of epileptiform discharges that produced a good EZ localization when averaged over long time intervals (approx. 60 min recording, see Figure 1E and 1F). Figures 2E and 2F show the DCE including all the events as gray dots and highlighting in color the epileptiform discharges pertaining to the cluster 09_09_09_05. Figures 2E and 2F show a clear oscillatory dynamics and rhythmic burst of events pertaining to the cluster 09_09_09_05, respectively. Importantly, Figures 2E and 2F show that 1) the occurrence of the epileptiform discharges (CoI: 09_09_09_05) is specific to the EZ (resulting in more dark red dots than blue dots) and 2) the rate of the epileptiform discharges in the EZ (density of the dark red dots) increases and decreases following the temporal evolution of the DCE with positive slope and negative slope, respectively. These two features can also be identified in the Figures 2G and 2H showing the mean discharges (ER)computed in a sliding epoch of 5 min in length and 90% overlap. The clinically relevant consequence of these observations is exemplified for two patients in the Figures 2I and 2J showing that the performance of EZ localization as quantified by the area under the precision and recall curve(AUPREC for EZ) follows the dynamics of the mean rate of epileptiform discharges. Values

fluctuate between close to perfect classification (which would correspond to an AUPREC = 1) and very small values close to chance level (gray filled circles in the Figures 2I and 2J). Importantly, we found that the observed temporal fluctuations of the IEDs rate entraining the precision to localize the EZ over fast-ultradian time scales occurs spontaneously during both the awake and the non-REM sleep states of the patients (see Appendix S1, Section 11). Moreover, the magnitude of the fluctuations of the AUPREC for EZ based on the rate of different subtypes of interictal events disclosed no significant differences at the group level between both awake vs non-REM sleep states, and also between two SEEG recording sessions taken at different days and time of day for the same patient state (awake at rest). For a detailed description of these results the reader is referred to the

Appendix S1, Sections 11 and 12. We also investigated the dependence of the observed fluctuations of the AUPREC for EZ on the type of events and on the specificity of the detector of interictal discharges (see Appendix S1, Sections 6 and 7). Figures 2I, 2J, 3A and 3B show that the events pertaining to the clusters 09_09_09_05, 0_09_09_05 and the Spike-like group produce similar temporal fluctuations of the AUPREC for EZ. These results reveal that the temporal dynamics of the events rate during interictal periods is present across different subtypes of epileptiform discharges and effectively entrains the precision to localize the EZ. Figures 3A and 3B show that, as expected, non-epileptic events (blue dots) produce very low values of AUPREC for EZ when compared to the epileptiform discharges (red dots), however, fluctuations of the AUPREC for EZ values are observed in both types of events. Figures 3E and 3F show the absolute difference (AD) between the extreme values (max - min) of the AUPREC for EZ time series based on the rate of IEDs, as a function of the sliding epoch length. Importantly, we found that the magnitude of the fast-ultradian fluctuations of the AUPREC for EZ based on the rate of IEDs decay exponentially as a function of the epoch length with a characteristic time and 3F). This scale-rich behavior is essentially different from the temporal dynamics of the AD of AUPREC for EZ based on the non-epileptic interictal events showing a scale -free trend (see Figures 3G and 3H and Appendix S1, Section 8). Besides, the non-epileptic interictal events were found to be significantly more abundant in the NIZ (see Figures S1C and S1D). Of note, the fluctuations of the rate of IEDs in EZ present a scale-free like dependence as a function of the epoch length (linear trend in a log-log plots shown in Figures S2I and S2J), which is different from the exponential trend with a characteristic time scale *Tao* disclosed by the fluctuations of the corresponding AUPREC for EZ (see the linear trend in the log-linear plots shown in Figures S2A, 3E and S2B, 3F). The latter, suggests that the observed fast-ultradian fluctuations of the AUPREC for EZ can not be completely explained by considering it simply as a function of the IEDs rate fluctuations within the EZ (see the caption of the Figure S2). Taken together, these results suggest that overlooking the spontaneous fast-ultradian dynamics of IEDs can produce incomplete and/or misleading information, leading to a suboptimal delineation of epileptogenic targets, and this holds true regardless of the specificity of the IEDs

detector included in the processing pipeline (compare the fluctuations disclosed by the clusters 0_09_09_05 and 09_09_09_05 with respect to the Spike-like group in the Figures 3A to 3D).

Putative mechanisms linked to the fast-ultradian dynamics of the rate of interictal events

The temporal fluctuation of the rate of IEDs in a given brain region can originate from variations in excitability within this region. However, it could also be explained - in a complementary way - by fluctuations in propagation from a primary irritative zone to a secondary zone. [28-30] In order to test the propagation hypothesis, we correlated the event rates between the EZ and the PZ (see Appendix S1, Section 5). It is important to note that the propagation of IEDs across macroscopic networks occurs within sub-second time scales (approx. 100 ms from temporal to frontal regions).[12,13] As a consequence, this fast propagation should not influence the measure of zero-lag correlation between event rates averaged over sliding epochs of several minutes in length (see Appendix S1, Section 5). Following this reasoningation mechanism in
order to quantitatively test this hypothesis over the fast-ultradian time scales: 1) the dynamics of the mean rate of IEDs in EZ should positively correlate with the dynamics of the mean rate of the same subtype of IEDs in PZ and 2) the AUPREC for EZ time series should negatively correlate with the dynamics of mean rate of IEDs in PZ (i.e., the occurrence of IEDs in PZ effectively impairs the EZ localization). Figure 4 shows the quantification of the two criteria associated with the propagation mechanism for three type of events and across three sliding epoch lengths. The percentage of patients satisfying the two criteria associated with the propagation mechanism is up to approx. 23% (8/35), 14% (5/35) and 11% (4/35) for epoch lengths of 1 min, 5 min and 10 min, respectively. These results strongly suggest that the propagation mechanism could have a dominant role in explaining the interictal fluctuations of the AUPREC for EZ time series only in a limited fraction of the analyzed patients. This suggests that the excitability of the epileptogenic tissues, along with other factors such as the brain state and the probed brain region, could play a more relevant role in explaining the spontaneous dynamics of the IEDs rate constraining the precision to localize the EZ over fast-

ultradian time scales. Further details related to the propagation mechanism are discussed in the Appendix S1, Section 9.

Predicting the spontaneous fast-ultradian dynamics to improve the epileptogenic zone localization

In this section we propose a strategy to prospectively estimate, i.e. without knowing the ground truth classification of EZ, the interictal epoch for near-optimal EZ localization based on IEDs rate. For this, we quantitatively define the optimal EZ localization for each patient as that corresponding to the maximum value of the AUPREC for EZ time series which is characterized by a temporal fluctuations over fast-ultradian time scales (see Figures 2I, 2J, 3A and 3B). Accordingly, the proposed method aims at estimating the time position of the sliding epoch corresponding to the maximum value of the AUPREC for EZ time series computed based on the rate of a given subtype of IEDs. The violin plot corresponding to the case "Best 5 min epoch (Max AUPREC)" shown in Figure 5D, summarizes the optimal EZ localization id IEDs pertaining to the cluster 09_09_09_05. We started by considering the fact that the interictal temporal dynamics of the AUPREC for EZ highly correlates with that associated with the mean rate of IEDs in EZ. Figures 2E to 2J illustrate this phenomenon for two particular patients (see also Figures S13 to S16 and S19 to S22). Moreover, Figures 5A and 5B show that the correlation between the two time series: AUPREC for EZ and "ER of IEDs (CoI: 09_09_09_05) in EZ", is positive and statistically significant in 77%(27/35) of the patients. Then, we investigated possible measures correlating with the AUPREC for
EZ time series and suitable to be applied in a prospective manner. This requires the measures to be independent of the EZ, PZ, NIZ ground truth classification of the SEEG channels. We found that the time series corresponding to the mean rate of events including all the clusters and averaged across all the channels (ER of all Clust in all Chan) negatively correlates with the AUPREC for EZ time series computed using these IEDs subtypes (e.g. clusters 0_09_09_05 and 09_09_09_05 associated by the epileptologists with interictal epileptiform spikes and spike-wave complexes respectively). Note that the overall rate of interictal events "ER of all Clust in all Chan" across all the SEEG channels is a

suitable measures for prospective analysis since they do not depend on the SEEG channels classification in EZ, PZ, NIZ. Figures 5B and 5C show that the correlation between the time series AUPREC for EZ (CoI: 09_09_09_05) and "ER of all Clust in all Chan", is negative and statistically significant in 63% (22/35) of the patients. A discussion regarding the putative mechanisms underlying this correlations is given in the Appendix S1, Section 10.

Based on these findings we estimated the epoch for near-optimal EZ localization as the interictal epoch corresponding to the minimum value of the "ER of all Clust in all Chan". For the IEDs corresponding to the cluster 09_09_09_05, Figures 5D, 5G and 5H show that the 5 min-epoch estimated in each patient using the proposed method produces at the population level an EZ localization slightly better than that obtained using the whole time series available in each patient (Bonferroni-adjusted $P = 0.084$, non-parameteric Wilcoxon signed rank test). Besides, these two cases (estimated best 5 min-epoch and whole time series) perform significantly worst and better than the cases for the actual best 5 min-epoch (i.e. maximum value of the AUPREC for EZ time series in each patient) and the wo€ for EZ time series in each patient), respectively (see Figures 5D and 5F to 5I). Figures 5E shows that the 5 min-epoch estimated in each patient using the proposed method produces an EZ localization at the population level significantly better with respect to that obtained with a 5 min epoch randomly sampled from the

interictal recordings of each patient ($P = 0.016$, 10^5 random samplings). Notably, we found that for the EZ and RZ localization using the cluster 09_09_09_05, the proposed method performs at the population level significantly better with respect to the approach based on a randomly sampled epoch, for epoch lengths in the range 5 - 10 min (in all the cases we obtained $P < 0.05$, 10^5 random samplings, see Figures 5 and S12). The predictive performance for near-optimal EZ and RZ localization of all the NODE clusters is discussed in the Appendix S1, Section 10 in connection with the Figures S8 to S11.

Discussion

Spontaneous fast-ultradian dynamics of the rate of interictal events

In this study, we show that the spontaneous dynamics of different subtypes of IEDs observed over fast-ultradian time scales emerge as an intrinsic feature of these EZ biomarkers, defined by the occurrence of amplitude outliers across frequency bands of interest (see Figure 1). This approach allowed us to investigate the temporal dynamics of a massive number of interictal events (see Figures 2A to 2D), including several subtypes of epileptiform discharges predominantly occurring in EZ as well as non-epileptic events associated with amplitude outliers in low frequency bands (1 Hz - 30Hz). These latter were found to be significantly less abundant in EZ with respect to NIZ (see Figure 1, S1 and S3). The analysis of the rate of these interictal events revealed underlying temporal dynamics characterized by sub-hour time scales which includes, but is not exclusive of, the IEDs observed in the EZ (compare Figures 2C vs 2D and Figures 2E vs 2F). Crucially, we found that the observed dynamics of the rate of events is an intrinsic feature of the interictal brain activity captured by the SEEG traces. Thatic events is not, or at least can not be explained solely by, an epiphenomenon associated with a particular parameters configuration of the NODE algorithm (see Figures S4, S5 and S6). We found that the NODE algorithm segregates the interictal epileptiform spikes visually marked by an epileptologist (FBo)into different sub-clusters (see Figure S3). Whereas most of visually marked spikes correspond to NODE clusters found to be significantly more abundant in EZ than in NIZ (e.g. 09_09_09_05,0_09_09_05), leading to a good EZ localization (see Figure S1), they showed different characteristics regarding their temporal dynamics. Firstly, we found that the rate of different types of interictal epileptogenic discharges undergo temporal fluctuations over fast-ultradian time scales as commonly examined in clinics. Previous studies have reported that the rate of interictal epileptic spikes increase during wakefulness and sleep,[10,14,15,17,18] and is suppressed during attention and memory tasks.[31-34] In contrast, the fast-ultradian temporal dynamics reported in this work was observed and characterized preoperatively in the interictal SEEG traces of 35 patients with Engel I seizure outcome and appears to occur spontaneously, that is, not triggered by or exclusively

associated with a particular cognitive task, wakefulness, sleep, seizure occurrence, post-ictal state or antiepileptic drug withdrawal (see subsection "Patients and intracerebral recordings" in Methods and Sections 11 and 12 of the Appendix S1). Secondly, we found that the minimization of the rate of interictal events (epileptic and non-epileptic) across all the SEEG channels is a good predictor of the interictal epoch (in the range 5 - 10 min in length) for near-optimal EZ localization based on specific subtypes of IEDs. Notably, we found that for the RZ localization based on the IEDs subtype 09_09_09_05, the proposed method performs at the population level significantly better than both 1) using the whole time series available in each patient and 2) using a short epoch (length ≈ 5 - 10 min) randomly sampled from the interictal recordings of each patient. Of note, this novel and counter-intuitive link between the dynamics of the overall rate of polymorphic events and the rate of specific subtypes epileptiform spikes which was exploited here to improve the EZ localization would be very difficult, if not impossible, to unveil by solely considering a limited subtype of events (e.g. visually marked epileptic spikes). Regarding the mechanisms underlying the observed fast-ultradian dynamics, our results suggest a dominant effect only in a limited fraction of the analyzed patients (see Figure 4), suggesting that the excitability of the epileptogenic tissue along with other factors such as the brain state and the probed brain region could play a more relevant role in explaining the spontaneous temporal dynamics of the IEDs rate entraining the precision to localize the EZ over sub-hour time scales.

Taken together, our results show that the rate of different subtypes of IEDs spontaneously undergoes temporal fluctuations which effectively constraint the precision to localize the EZ over fast-ultradian time scales as commonly analyzed in clinics,[5,8] hence, representing a clinically relevant factor for surgical planning in drug-resistant epilepsy.

Limitations

Whereas all the patients included in the study where seizure-free after surgery, indicating that the analyzed SEEG traces effectively capture the brain activity associated with EZ, further investigation

is warranted to disentangle the observed dynamics of interictal events from the heterogeneity and variable number of explored brain regions. Besides, given the heterogeneous exposure to antiepileptic drugs of the analyzed patients, further investigation is required to assess the effect of this factor on the fast-ultradian dynamics of the rate of interictal events. Importantly, the possibility that the fast-ultradian fluctuations of the rate of interictal events analyzed in this work could vary with or be hierarchically coupled to another rhythms with longer time periods (e.g. circadian rhythms), deserve further investigation. However, this does not change the conclusions of our study regarding the existence of the fast-ultradian fluctuations of the rate of interictal events entraining the presicion to localize the EZ, and its importance for surgical planning in drug-resistant epilepsy.

Conclusion

A major limitation of previous works assessing the performance of epileptogenic biomarkers like interictal spike and HFOshe time-varying factors
underlying the genesis of these biomarkers.[5,8,9,26,27] This limitation can effectively produce incomplete and/or misleading information, leading to a suboptimal delineation of epileptogenic targets. In this study, we provided for the first time a method to investigate and predict the spontaneous fast-ultradian dynamics of interictal transient event-like biomarkers. Based on our results, the recommendation for clinical applications is that an interictal time interval of at least 30 min in length is required to stabilize the findings, i.e. in order to produce a relative attenuation of 90% of the AUPREC for EZ fluctuations with respect to that observed in the case of a 5 min interictal time window (see the calculations in Appendix S1, Section 8). The proposed method for polymorphic events analysis paves the way to prospectively estimate the interictal time interval for near-optimal EZ localization in a substantial fraction of the analyzed patients based solely on the dynamics of the intracranial recordings (see Figure 5B). This fact reveals a novel and counter-intuitive link between the fast-ultradian dynamics of the overall rate of polymorphic events (epileptic and non-epileptic) and the rate of specific subtypes of epileptiform spikes as an intrinsic feature of

the interictal brain activity (see Figures 5 and S7 to S12). This result is clinically relevant as we showed how it can be exploited to improve the EZ localization and also offer a novel approach to investigate the time-varying factors underlying the genesis of different subtypes of IEDs.

References

1 Guery D, Rheims S. Clinical Management of Drug Resistant Epilepsy: A Review on Current Strategies. Neuropsychiatr Dis Treat. 2021 Jul 12; 17:2229-2242. DOI: 10.2147/NDT.S256699.

2 Baud MO, Rao VR. Gauging seizure risk. Neurology. 2018 Nov 20; 91(21):967-973. DOI: 10.1212/WNL.0000000000006548.

3 Jobst BC, Bartolomei F, Diehl B, et al. Intracranial EEG in the 21st Century. Epilepsy Curr. 2020 Jul; 20(4):180-188. DOI: 10.1177/1535759720934852.

4 Bartolomei F, Lagetworks: Contribution of SEEG and signal analysis. Epilepsia. 2017 Jul; 58 (7):1131-1147. DOI: 10.1111/epi.13791.

5 Bartolomei F, Trebuchon A, Bonini F, et al. What is the concordance between the seizure onset zone and the irritative zone? A SEEG quantified study. Clin Neurophysiol 2016, 127:1157 - 1162. DOI: 10.1016/j.clinph.2015.10.029.

6 Sharma NK, Pedreira C, Centeno M, et al. A novel scheme for the validation of an automated classification method for epileptic spikes by comparison with multiple observers. Clin Neurophysiol. 2017 Jul, 128(7):1246-1254. DOI: 10.1016/j.clinph.2017.04.016.

7 Ren L, Kucewicz MT, Cimbalnik J, et al. Gamma oscillations precede interictal epileptiform spikes in the seizure onset zone. Neurology. 2015 Feb 10; 84(6):602-8. DOI: 10.1212/WNL.0000000000001234.

8 Roehri N, Pizzo F, Lagarde S, et al. High-frequency oscillations are not better biomarkers of epileptogenic tissues than spikes. Ann Neurol. 2018 Jan;83(1):84-97. DOI: 10.1002/ana.25124.

9 Thomas J, Kahane P, Abdallah C, et al. A Subpopulation of Spikes Predicts Successful Epilepsy Surgery Outcome. Ann Neurol. 2022 Nov 13. DOI: 10.1002/ana.26548.

10 Conrad EC, Tomlinson SB, Wong JN, et al. Spatial distribution of interictal spikes fluctuates over time and localizes seizure onset. Brain. 2020 Feb 1, 143(2):554-569. DOI: 10.1093/brain/awz386.

11 Badier JM, Chauvel P. Spatio-temporal characteristics of paroxysmal interictal events in human temporal lobe epilepsy. J Physiol Paris. 1995; 89(4-6):255-64. DOI: 10.1016/0928-4257(96)83642-4.

12 Tomlinson SB, Wong JN, Conrad EC, Kennedy BC, Marsh ED. Reproducibility of interictal spike propagation in children with refractory epilepsy. Epilepsia. 2019 May, 60(5):898-910. DOI: 10.1111/epi.14720.

13 Azeem A, von Ellenrieder N, Hall J, Dubeau F, Frauscher B, Gotman J. Interictal spike networks predictfocal epilepsy. Ann Clin Transl Neurol. 2021 Jun, 8(6):1212-1223. DOI: 10.1002/acn3.51337.

14 Spencer SS, Goncharova II, Duckrow R B, Novotny EJ, Zaveri HP. Interictal spikes on intracranial recording: behavior, physiology, and implications. Epilepsia. 2008 Nov, 49(11):1881-92. DOI: 10.1111/j.1528-1167.2008.01641.x.

15 Karoly PJ, Freestone DR, Boston R, et al. Interictal spikes and epileptic seizures: their relationship and underlying rhythmicity. Brain. 2016 Apr, 139(Pt 4):1066-78. DOI: 10.1093/brain/aww019.

16 Baud MO, Kleen JK, Mirro EA, et al. Multi-day rhythms modulate seizure risk in epilepsy. Nat Commun. 2018 Jan 8, 9(1):88. DOI: 10.1038/s41467-017-02577-y.

17 Seneviratne U, Lai A, Cook M, D'Souza W, Boston RC. "Sleep Surge": The impact of sleep onset and offset on epileptiform discharges in idiopathic generalized epilepsies. Clin Neurophysiol. 2020 May, 131(5):1044-1050. DOI: 10.1016/j.clinph.2020.01.021.

18 Lambert I, Tramoni-Negre E, Lagarde S, et al. Accelerated long-term forgetting in focal epilepsy: Do interictal spikes during sleep matter? Epilepsia. 2021 Mar, 62(3):563-569. DOI: 10.1111/epi.16823.

19 Gerkema, M.P. (2002). Ultradian Rhythms. In: Kumar, V. (eds) Biological Rhythms. Springer, Berlin, Heidelberg. DOI: 10.1007/978-3-662-06085-8_17

20 Bancaud J, Angelergues R, Bernouilli C, Bonis A, Bordas-Ferrer M, Bresson M, Buser P, Covello L, Morel P, Szikla G, Takeda A, Talairach J. Functional stereotaxic exploration (SEEG) of epilepsy. Electroencephalogr Clin Neurophysiol. 1970 Jan, 28(1):85-6.

21 Bartolomei F, Chauvel P, Wendling F. Epileptogenicity of brain structures in human temporal lobe epilepsy: a o8 Jul; 131(Pt 7):1818-30.
DOI: 10.1093/brain/awn111.

22 Bradley Efron (2004) Large-Scale Simultaneous Hypothesis Testing, Journal of the Am Statist Association, 99:465, 96-104, DOI: 10.1198/016214504000000089.

23 Bradley Efron. Size, power and false discovery rates. Ann. Statist. 35 (4) 1351-1377, August 2007. DOI: 10.1214/009053606000001460.

24 Gançarski P., Dao TBH., Crémilleux B., Forestier G., Lampert T. (2020). Constrained Clustering: Current and New Trends. In: Marquis, P., Papini, O., Prade, H. (eds) A Guided Tour of Artificial Intelligence Research. Springer, Cham. DOI: 10.1007/978-3-030-06167-8_14.

25 Roehri N, Lina JM, Mosher JC, Bartolomei F, Benar CG. Time-Frequency Strategies for Increasing High-Frequency Oscillation Detectability in Intracerebral EEG. IEEE Trans Biomed Eng. 2016 Dec; 63(12):2595-2606. DOI: 10.1109/TBME.2016.2556425.

26 Motoi H, Miyakoshi M, Abel TJ, et al. Phase-amplitude coupling between interictal high-frequency activity and slow waves in epilepsy surgery. Epilepsia. 2018 Oct, 59(10):1954-1965. DOI: 10.1111/epi.14544.

27 Pizzo F, Roehri N, Medina Villalon S, et al. Deep brain activities can be detected with magnetoencephalography. Nat Commun 10, 971 (2019). DOI: 10.1038/s41467-019-08665-5.

28 Penfield W, Jasper H. Epilepsy and the functional anatomy of the human brain. London: J. & A. Churchill; 1954.

29 Jasper HH, Arfel-Capdeville G, Rasmussen T. Evaluation of EEG and cortical electrographic studies for prognosis of seizures following surgical excision of epileptogenic lesions. Epilepsia 1961, 2:130 - 7. DOI: 10.1111/j.1528-1157.1942.tb00405.x.

30 Köksal-Ersöz E, Lazazzera R, Yochum M, et al. Signal processing and computational modeling for interpretation of SEEG-recorded interictal epileptiform discharges in epileptogenic and non-epileptogenicl088/1741-2552/ac8fb4.

31 Meisenhelter S, Quon RJ, Steimel SA, et al. Interictal Epileptiform Discharges are Task Dependent and are Associated with Lasting Electrocorticographic Changes. Cereb Cortex Commun. 2021 Mar 20, 2(2):tgab019. DOI: 10.1093/texcom/tgab019.

32 Quon RJ, Meisenhelter S, Adamovich-Zeitlin RH, et al. Factors correlated with intracranial interictal epileptiform discharges in refractory epilepsy. Epilepsia. 2021 Feb;62(2):481-491. DOI: 10.1111/epi.16792.

33 Henin S, Shankar A, Borges H, et al. Spatiotemporal dynamics between interictal epileptiform discharges and ripples during associative memory processing. Brain. 2021 Jun 22;144(5):1590-1602. DOI: 10.1093/brain/awab044.

34 Matsumoto JY, Stead M, Kucewicz MT, et al. Network oscillations modulate interictal epileptiform spike rate during human memory. Brain. 2013 Aug, 136(Pt 8):2444-56. DOI: 10.1093/brain/awt159.

Supporting information

Additional Supporting Information may be found in the online version of this article:

Appendix S1. Supplementary methods and results.

Tables

Table 1: Patients clinical information. All the 35 patients (20 women and 15 men) have Engel I seizure outcome classification at least 12 months after the surgical procedure. The information regarding the resected zone was not available for the patient 13. The time of day (or night) when the SEEG recordings were made and the length of the interictal SEEG traces corresponding to these patients can be found in the Table S1 of the Appendix S1. To ensure the anonymity, serial numbers attributed randomly to each patient are used as patients ID. The resulting ID numbers have no correlation with any clinical information of the patients.

Patient ID	Age at SEEG	Sex	EZ localization	Etiology
1	36-40	M	Temp - Fr	FCD
2	26-30	F	Temp	GG
3	41-45	F	Temp	HS
4	16-20	M	Fr	G
5	21-25	F	SMA	FCD
6	26			HS
7	26-30	F	Temp	HS
8	26-30	F	Par	FCD
9	41-45	M	Ins	N/A
10	26-30	M	Fr	G
11	56-60	M	Temp - Fr	FCD
12	41-45	M	Temp - Fr	G
13	41-45	F	pre Mot	FCD
14	11-15	M	Mot - pre Mot	Stroke
15	51-55	F	right Op and Pos Ins	FCD
16	1-5	M	Occ	GG
17	11-15	F	Fr	TS
18	56-60	M	left Temp Lat and Par	HS
19	36-40	F	right Mes - Temp	HS
20	6-10	F	left Fr	Neonatal ACV
21	46-50	M	right Ant MesTemp and Ins	HS
22	11-15	M	left Temp - Mes	DNET
23	11-15	F	left Temp Basal and left Temp - Occ	Neonatal ACV

24	66-70	M	left Temp - Mes	HS
25	11-15	M	left Hem	N/A
26	31-35	F	left Temp - Mes	G
27	6-10	M	left Temp - Mes	HS
28	11-15	F	right Fr	FCD
29	21-25	F	right Lat Temp	Non-specific
30	46-50	F	left Temp - Mes	Non-specific
31	36-40	F	Temp Lat	GG
32	21-25	F	Temp Lat	FCD
33	21-25	F	Par	DNET
34	31-35	F	Temp - Mes	HS + FCD
35	21-25	F	Fr	FCD

Symbols and abbreviations: F, Female; M, Male; Temp, Temporal lobe; Fr, Frontal lobe; Par, Parietal lobe; Occ, Occipital lobe; SMA, Supplementary motor area; Ins, Insular; Mot, Motor cortex; Op, Opercular; Ant, Anterior; Pos, Posterior; Lat, Lateral; Mes, Mesial; Hem, Hemisphere; FCD: Focal cortical dysplasia; GG, Ganglioglioma; HS, Hippocampal sclerosis; N/A, Not available; G, Gliosis; TS, Tuberous sclerosis; DNET: Dysembryoplastic neuro-ep; NO, Not operated.

Figure legends

Figure 1: Nested Outlier Detection (NODE) algorithm. (A) Schematic representation of the filtering and thresholding stages of the NODE algorithm together with the resulting 4-digit labels assigned to the detected events. **(B, C, D)** Raw time series and whitened time-frequency maps (scalograms using Morlet wavelets) for three clusters of events detected in the EZ (B: Hippocampus cephalis) of the patient 7. **(E, F, G)** Mean rate of events in each bipolar channel obtained from the whole interictal SEEG recording available for the patient 7 (60 min). The insets included in panels **(E)** and **(F)** show the results of the precision and recall analysis for the IEDs subtypes 09_09_09_05 (F1 max = 0.93) and 0_09_09_05 (F1 max = 0.73). The chance level corresponding to a random classifier, was computed as the ratio between the number of channels pertaining to EZ and the total number of channels in each patient (black dashed line). Symbols and abbreviations: NODE, Nested Outlier Detection; PSD, power spectral density; EZ, epileptogenic zone; PZ, propagation zone; NIZ, non-involved zone; PPV, P, Temporal pole; A,Amygdala complex; B, Hippocampus cephalis; C, Hippocampus caudalis; TB, Temporal basalis; I,Insula; H, Gyrus temporal transverse Heschl; OP, Opercule parietal; OF, Opercule frontal; FT, Front Triangularis; OR, Fronto Orbitaire oblique.

Figure 2: Spontaneous temporal dynamics of the rate of interictal events. (A, B) Cumulative count of events including all events subtypes (epileptic and non-epileptic) detected by the NODE algorithm (80 clusters). Each line correspond to a single bipolar channel and the slope of each line (number of events / time) is the mean rate of events for that particular SEEG channel. **(C, D)** Detrended cumulative count of events (cumulative residual). **(E, F)** Cumulative residual showing all the detected events (gray dots) and the discharges pertaining to the cluster 09_09_09_05 in color (NIZ: blue dots, PZ: light red dots, EZ: dark red dots). **(G, H)** Mean rate of events pertaining to the cluster 09_09_09_05. The dots correspond to the mean value of the events rate at each time position of the sliding epoch of 5 min in length and 90% overlap. The shaded error bars correspond to the

standard error. **(I, J)** AUPREC for EZ localization based on the rate of events pertaining to the cluster 09_09_09_05 at each time position of the 5 min length sliding epoch. Symbols and abbreviations: CoI, cluster of interest; EZ, epileptogenic zone; PZ, propagation zone; NIZ, non-involved zone; ER, events rate; AUPREC, area under the precision and recall curve.

Figure 3: Temporal dynamics of the goodness of EZ localization as quantified by the AUPREC based on the rate of interictal events. (A, B) Temporal evolution of the AUPREC for EZ localization based on the rate of IEDs (CoI: 0_09_09_05, Spike-like) and non-epileptic events (CoI: 09_09_0_0) computed using a sliding epoch of 5 min in length and 90% overlap. **(C, D)** Violin plots including all the patients paired across two CoIs showing the relative difference (RD) between the extreme values ((max - min) / max) of the AUPREC for EZ time series for three lengths of the sliding epoch (1 min, 5 min, 10 min). In all the cases, the overlap of the sliding epoch was 90% and it sweeps the whole interictal period available in each patient. In an inter-group paired analysis, the reported P values indicate lengths (Wilcoxon signed rank test with the P values Bonferroni-adjusted to correct for multiple comparisons across the
3 epoch lengths). In an intra-group paired analysis, only the 5 min epoch length in panel **(C)** presents significant difference between the distributions corresponding to CoI: 0_09_09_05 and Spike-like (P = 0.01, Wilcoxon signed rank test). **(E, F)** Log-linear plots showing the absolute difference (AD) between the extreme values (max - min) of the AUPREC for EZ based on the rate of IEDs as a function of the sliding epoch length. The red line and red shaded error bars represent the linear regression and the 95% confidence interval, respectively. These linear trends in the log-linear plots suggest an exponential dependence $y \propto e^{-x/Tao}$ where y represents the AD of AUPREC for EZ being proportional to a decaying exponential function of the epoch length x, with a characteristic time scale *Tao*. For CoI: 0_09_09_05 (panel E) we obtain: Slope = -0.079 [1/min] (*Tao* = 12.7 [min]), SE =0.002 [1/min], P < 0.001, t-statistic of the two-sided hypothesis test. For CoI: 09_09_09_05 (panel F)we obtain: Slope = -0.086 [1/min] (*Tao* = 11.7 [min]), SE = 0.002 [1/min], P < 0.001, t-statistic of the two-sided hypothesis test. The AD of AUPREC for EZ presents a linear dependence in a log-linear

plot suggesting an exponential trend, with a characteristic time scale *Tao*. **(G, H)** Log-log plots showing the AD of AUPREC for EZ based on the rate of the non-epileptic events as a function of the sliding epoch length. The AD of AUPREC for EZ presents 2 linear segments with different behavior below and above ≈ 10 min epoch length. This linear dependence in a log-log plot suggests a scale-free dynamics. Symbols and abbreviations: CoI, cluster of interest; IEDs, interictal epileptogenic discharges; EZ, epileptogenic zone; PZ, propagation zone; NIZ, non-involved zone; AD, absolute difference; AUPREC, area under the precision and recall curve.

Figure 4: Testing the hypothesis that the temporal fluctuations of the AUPREC for EZ on fast-ultradian time scales are associated with the propagation of IEDs from EZ to PZ. Panels **(A)**, **(B)** and **(C)** correspond to the clusters 09_09_09_05, 0_09_09_05 and Spike-like, respectively. In each panel, the violin plots show all the patients paired across two correlations (ER of CoI in EZ vs ER of CoI in PZ) and (AUPREC for EZ vs ER of CoI in PZ). The three time series involved in the correlations (ER of CoI i computed using sliding epoch of length 1 min (left panel), 5 min (central panel) and 10 min (right panel) and 90% overlap scanning the whole interictal period available in each patient. Dotted gray lines correspond to

patients in which at least one of the two correlations result no significant. Dashed gray lines correspond to patients in which the two correlations are significant, but the signs of the correlations do not satisfy the criteria associated with the propagation hypothesis (see discussion in the text). Solid black lines correspond to patients in which the two correlations are significant and satisfy the criteria associated with the propagation hypothesis (see discussion in the text). The fractional number accompanying each paired violin plot indicates the fraction of patients satisfying all the criteria associated with the propagation hypothesis. The statistical significance of the correlations ($P < 0.05$) was assessed by using the Student's t distributions of the two-tailed hypothesis test under the null hypothesis that the correlation is zero. Symbols and abbreviations: CoI, cluster of interest; IEDs, interictal epileptogenic discharges; EZ, epileptogenic zone; PZ, propagation zone; NIZ, non-involved

zone; ER, events rate; AUPREC, area under the precision and recall curve; ER of CoI in EZ/PZ, mean rate of events pertaining to the CoI averaged over the EZ/PZ channels.

Figure 5: Estimating the best interictal 5 min-epoch for near-optimal EZ localization. (A) Scatter plot showing the correlation between the time series AUPREC for EZ and ER of CoI in EZ. **(C)** Scatter plot showing the correlation between the time series AUPREC for EZ and ER of all Clust in all Chan. In panels **(A)** and **(C)**, all the measures were computed for the CoI: 09_09_09_05 and each dot correspond to the measure value in a particular time position of the sliding epoch of 5 min in length and 90% overlap, covering the whole interictal SEEG time series available in each patient. The red line and red shaded error bars represent the linear regression and the 95% confidence interval, respectively. For panel **(A)** we obtained: Slope = +0.519 [1/min], SE = 0.020 [1/min], $P < 0.001$, t-statistic of the two-sided hypothesis test. For panel **(C)** we obtained: Slope = -0.334 [1/min], SE = 0.022 [1/min], $P < 0.001$, t-statistic of the two-sided hypothesis test. **(B)** Violin plots showing all the patients paired acr of CoI in EZ, and 2)AUPREC for EZ vs ER of all Clust in all Chan. Dotted gray lines correspond to patients in which at

least one of the two correlations is no significant. Dashed gray lines correspond to patients in which the two correlations are significant and, negative in the red violin plot and positive in the green violin plot, or have the same sign. Solid black lines correspond to patients in which the two correlations are significant and, positive in the red violin plot and negative in the green violin plot. The three fractional numbers accompanying the paired violin plots indicate the fraction of patients presenting significant value for the left-hand, both and right-hand correlations. The statistical significance of the correlations ($P < 0.05$) was assessed by using the Student's t distributions of the two-tailed hypothesis test under the null hypothesis that the correlation is zero. **(D)** Violin plots showing all the patients paired across the values of AUPREC for EZ based on a random classifier, computed as the ratio between the number of channels pertaining to EZ and the total number of channels in each patient (blue violin plot), and the AUPREC for EZ based on the rate of events pertaining to the cluster 09_09_09_05 (red violin plot). In an intra-group paired analysis (Wilcoxon signed rank test),

the reported P values indicate significant differences between the two distributions of AUPREC values in all the four cases shown. In an inter-group paired analysis, we found significant differences ($P < 0.001$) between all but one group pair: Estimated best 5 min epoch vs Whole time series ($P = 0.084$, Wilcoxon signed rank test with the P values Bonferroni-adjusted to correct for multiple comparisons across the 4 cases). **(E)** Histogram showing the distribution of the relative difference of the AUPREC for EZ with respect to the chance level (CL) for a 5 min epoch randomly sampled from the interictal SEEG recordings of each patient (10^5 random samplings). The CL was computed as the ratio between the number of channels pertaining to EZ and the total number of channels in each patient. The red vertical solid line shown in the histogram indicates the relative difference value corresponding to the estimated best 5 min epoch for near-optimal EZ localization (second case from the left in panel **D**). **(F, G, H, I)** Scatter plots corresponding to the four cases shown in panel **(D)**. In panels D, E and G, the estimated best 5 min epoch for near-optimal EZ localization corresponds to the interictal epoch producing the minimum value of ER of all Clust in all Chan. Symbols and abbreviations: CoI, clustee; AUPREC, area under the precision and recall curve. ACL, above chance level; ER of CoI in EZ/PZ, mean rate of events pertaining to the CoI averaged over the EZ/PZ channels; ER of all Clust in all Chan, mean rate of events including all the clusters and averaged across all the channels.

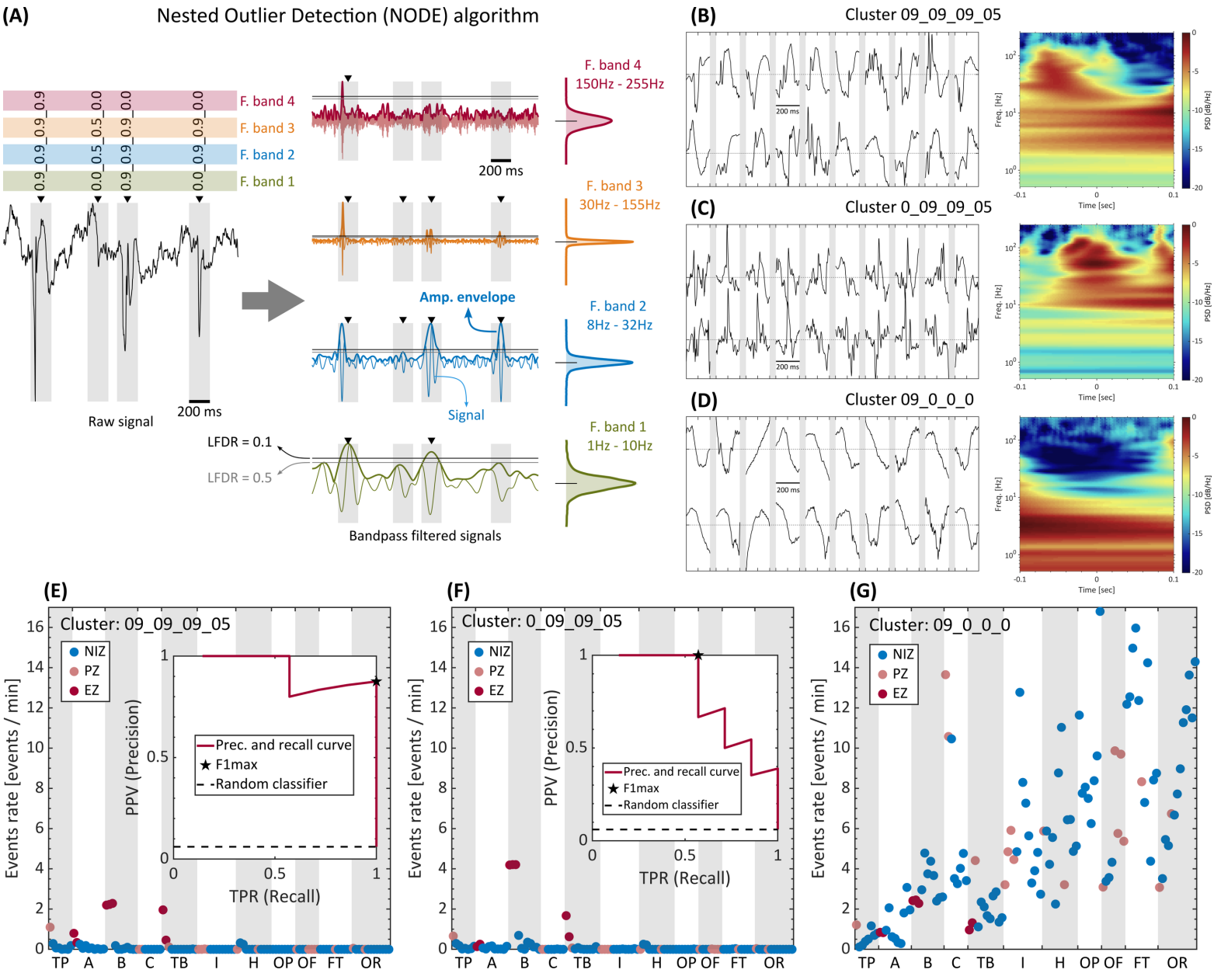

dellavale_figure_1_v2b_epilepsia_600dpi.tif

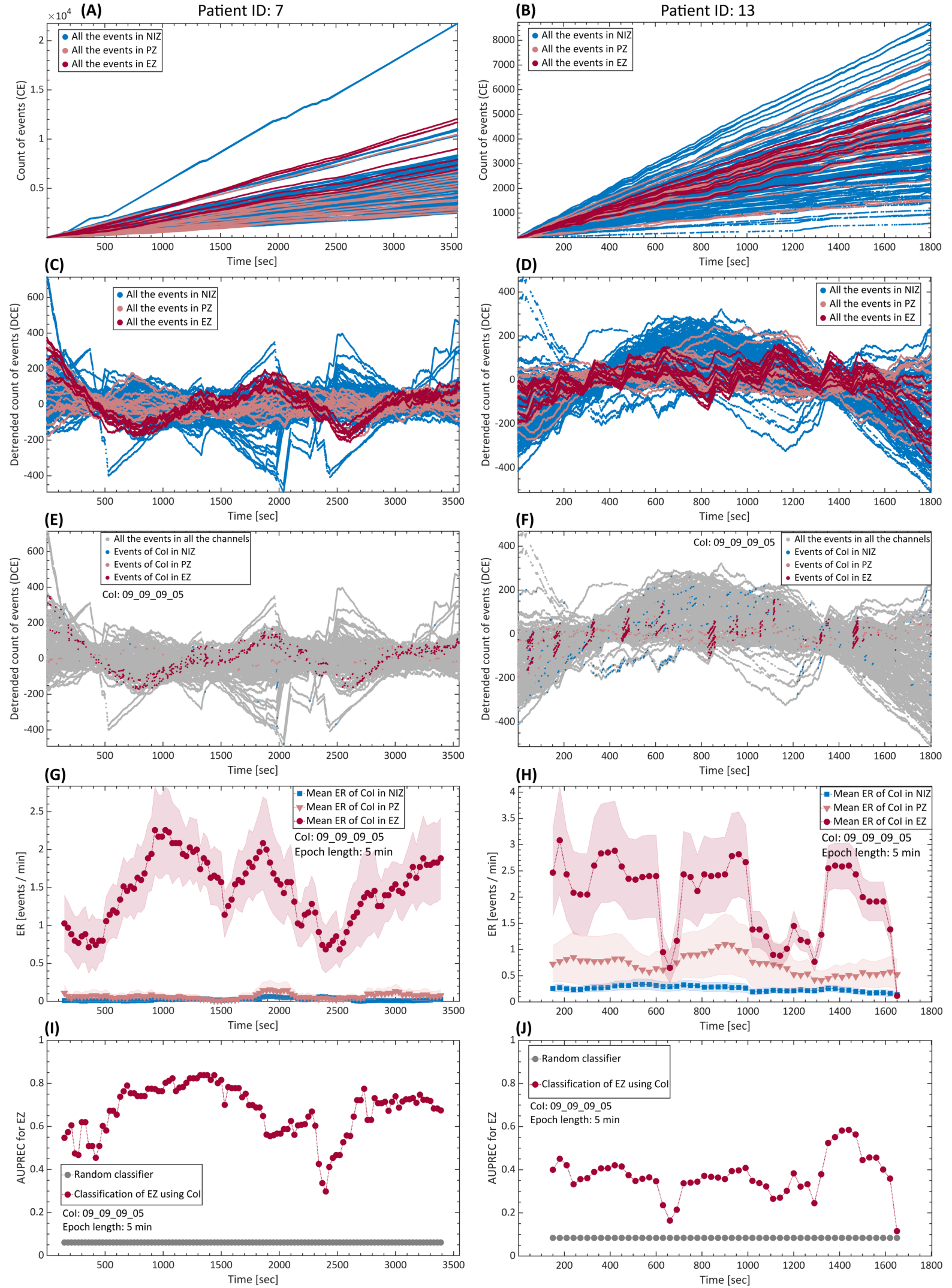

dellavale_figure_2_v2_epilepsia_600dpi.tif

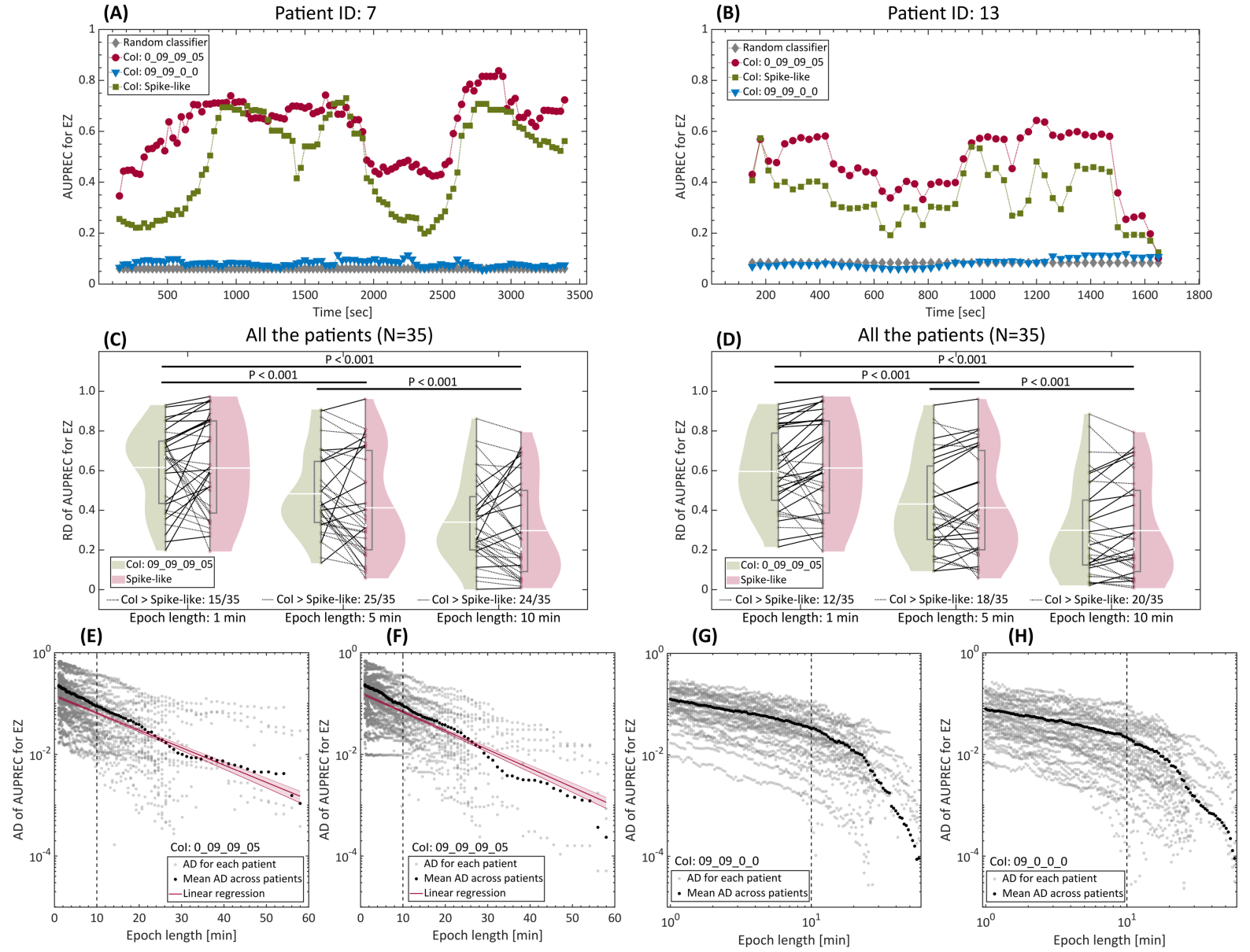

dellavale_figure_3_v3c_epilepsia_600dpi.tif

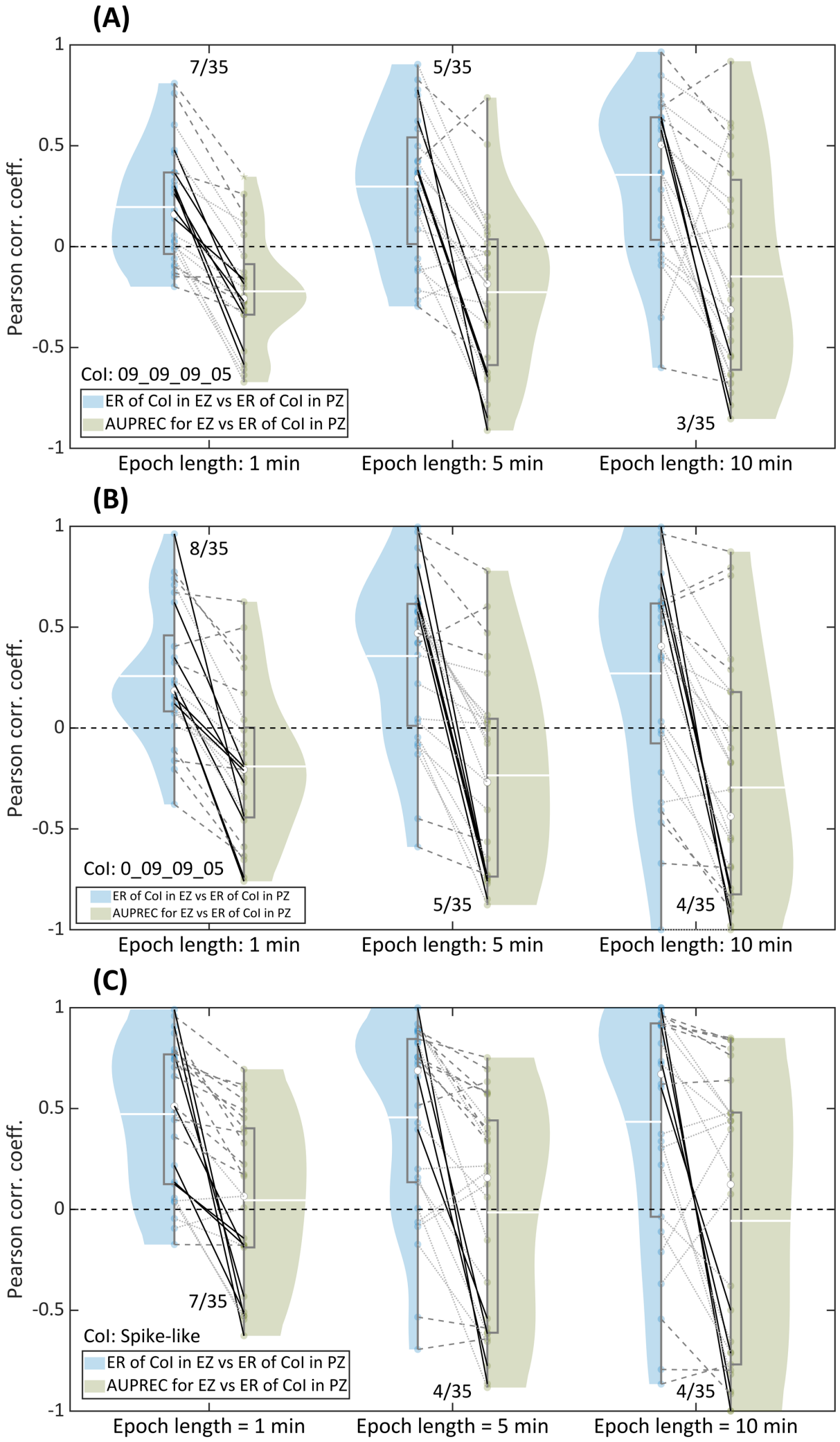

dellavale_figure_4_v2_epilepsia_600dpi.tif

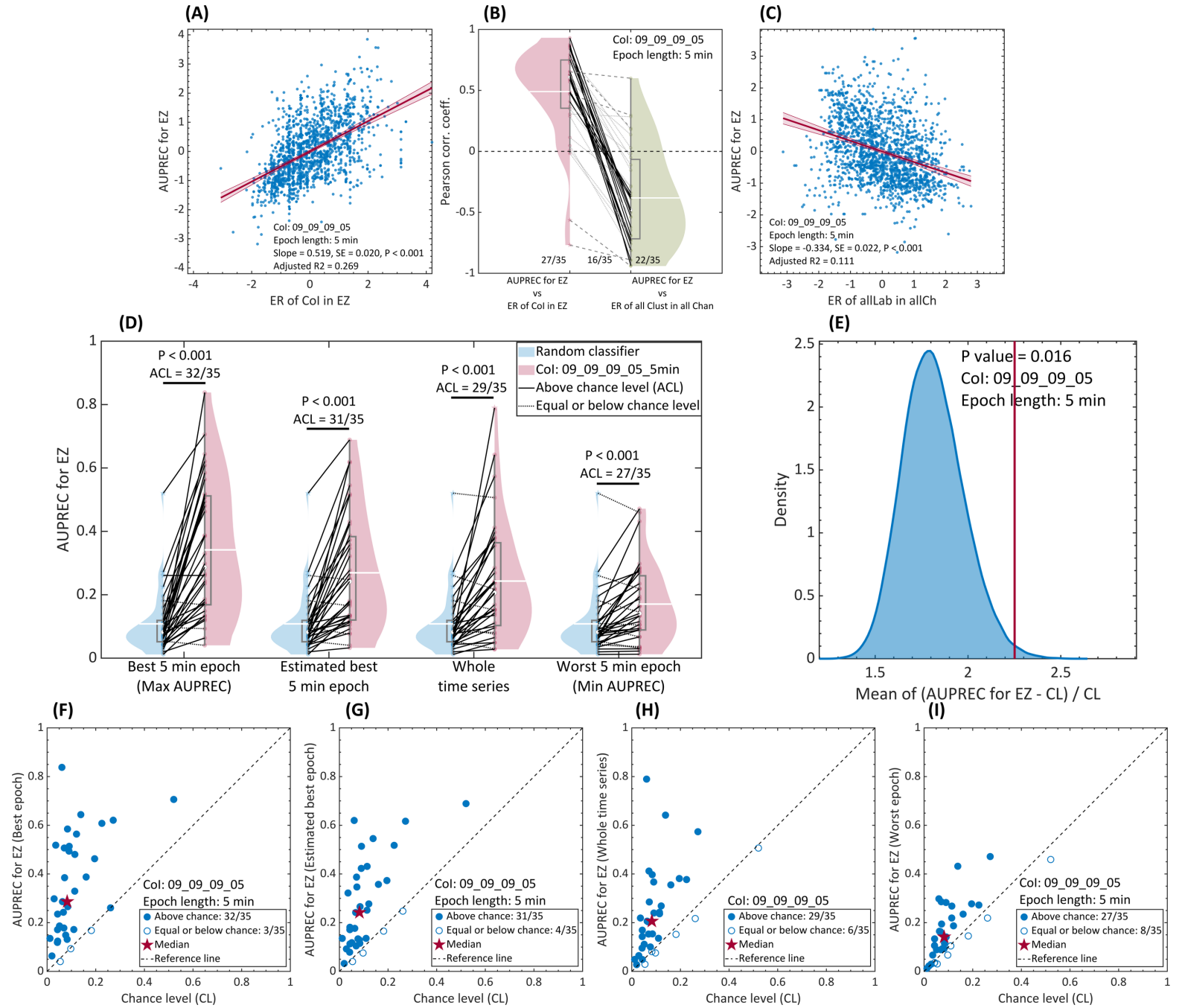

dellavale_figure_5_v1c_epilepsia_600dpi.tif